Paired Pulse Basis Functions for the Method of Moments EFIE Solution of Electromagnetic Problems Involving Arbitrarily-shaped, Three-dimensional Dielectric Scatterers

Anne I. Mackenzie[1], Sadasiva M. Rao[2], and Michael E. Baginski[3]

[1]Electromagnetics & Sensors Branch, NASA Langley Research Center, Hampton, VA 23681
a.i.mackenzie@larc.nasa.gov

[2]Electrical & Computer Engineering Department, Auburn University, Auburn, AL 36849
raosada@auburn.edu

[3]Electrical & Computer Engineering Department, Auburn University, Auburn, AL 36849
baginme@auburn.edu

Abstract — **A pair of basis functions is presented for the surface integral, method of moment solution of scattering by arbitrarily-shaped, three-dimensional dielectric bodies. Equivalent surface currents are represented by orthogonal unit pulse vectors in conjunction with triangular patch modeling. The electric field integral equation is employed with closed geometries for dielectric bodies; the method may also be applied to conductors. Radar cross section results are shown for dielectric bodies having canonical spherical, cylindrical, and cubic shapes. Pulse basis function results are compared to results by other methods.**

Index Terms — **electromagnetic scattering, basis functions, method of moments, dielectric, conducting, EFIE.**

I. INTRODUCTION

This work extends the use of a pair of orthogonal basis functions introduced in [1] for the determination of surface currents on a three-dimensional, arbitrarily-shaped electromagnetic scatterer. In [1], a solution method was demonstrated for perfect electric conductors (PEC) using unit pulse basis vectors; in this work, the method is further developed to include dielectric bodies.

Rao, Wilton, and Glisson (RWG) developed the RWG basis functions for method of moments (MoM) conducting body solutions in conjunction with triangular patch surface modeling [2]. Numerous other basis functions have been used for MoM solutions, including rooftop [3], wavelet [4], and Trintinalia-Ling [5] functions for specialized applications. However, for "all-purpose" modeling of arbitrarily-shaped, three-dimensional scatterers, the RWG basis functions remain in very wide usage. We propose that for lossy dielectric or dielectric (material) bodies, a pair of orthogonal basis functions should be more suitable in that the basis functions represent equivalent surface electric and magnetic currents

also defined as orthogonal to each other in each triangular patch. Improved solution reliability and accuracy should result from orthogonal basis functions, which produce strongly diagonal, well conditioned impedance matrices. In addition, the pulse basis vector functions are particularly simple in concept and in definition, which makes them attractive to explore. Orthogonal pulse basis functions are easier to implement in code than, for example, $\hat{n} \times$ RWG basis functions [6], $\hat{n}$ defined as the unit outward normal vector. The paired pulse basis vector solution method may be extended to include collections of scatterers, composite dielectric/conducting bodies, or bodies composed of numerous regions of constant permittivity and permeability.

II. PROBLEM FORMULATION

E_1, H_1

μ_1, ε_1

E_2, H_2
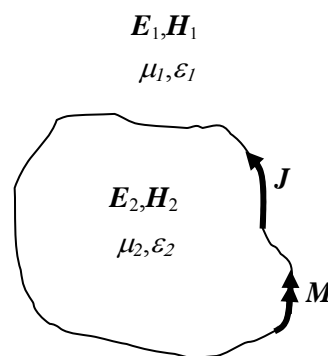
μ_2, ε_2

J

M

Fig. 1.   Arbitrarily-shaped, three-dimensional scatterer.

Considering the dielectric scatterer to be illuminated by an external source, we label the outer and inner regions of the scatterer as 1 and 2, respectively, shown in Fig. 1. We

apply the Equivalence Principle and enforce the continuity of the tangential **E**-field across the boundary surface S to write

$$\left[E_1^S(J) + E_1^S(M) + E^i \right]_{\text{tan}} = 0 \qquad (1)$$

just inside the surface and

$$\left[E_2^S(-J) + E_2^S(-M) \right]_{\text{tan}} = 0 \qquad (2)$$

just outside the surface. The superscript s and i refer to scattered and incident fields. J and M are the equivalent electric and magnetic surface currents residing on S. The scattered tangential electric field in (1) or (2) is given by the electric field integral equation (EFIE) as:

$$E^S = -j\omega A - \nabla \Phi - \nabla \times \frac{1}{\varepsilon} F \qquad (3)$$

where A is the magnetic vector potential,

$$A = \frac{\mu}{4\pi} \int_S J \cdot G \, dS , \qquad (4)$$

Φ is the electric scalar potential, $\Phi = \dfrac{-1}{j\omega\mu\varepsilon} \nabla \bullet A$, (5)

F is the electric vector potential,

$$F = \frac{\varepsilon}{4\pi} \int_S M \cdot G \, dS , \qquad (6)$$

G is the Green's function, $G = \dfrac{e^{-j\beta R}}{R}$, (7)

β is the phase constant, $\dfrac{2\pi}{\lambda}$, (8)

R is the distance between source and observation points, ε is electric permittivity, and μ is magnetic permeability.

(1) and (2) are rewritten by expanding J and M in all vector and scalar potential terms as pulse basis functions and incorporating the regions' respective values for ε and μ. For a closed triangular mesh containing N edges, the expanded MoM matrix equation contains a $2N$ x $2N$ impedance matrix to solve for N values of J and N values of M. These surface currents may then be used to calculate the radar cross section (RCS) from any observation angle.

III. NUMERICAL SOLUTION PROCEDURE

A. Basis Functions

Within each pair of adjacent triangular patches T_n^+ and T_n^-, the basis vectors for J_n and M_n are f_n and g_n, defined to be normal and parallel to the nth edge, respectively, as shown in Fig. 2. The basis vector functions have unit value and exist only in the shaded source regions, which need not be coplanar. These regions comprise two thirds of the area of the T_n^+ and T_n^- triangles. Plus and minus names have been assigned to designate the direction of electric current flow from plus to minus.
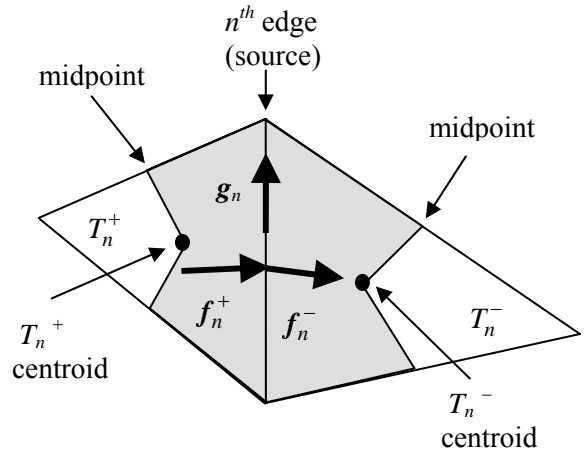

Fig. 2.   Unit pulse basis vectors f and g drawn for the nth edge; the surface currents J_n and M_n will be calculated normal and parallel to the edge, respectively.

At the nth edge,

$$J_n = \alpha_n(f_n^+ + f_n^-) \qquad (9)$$

$$M_n = \gamma_n(g_n) \qquad (10)$$

where α_n and γ_n are the expansion coefficients to be determined. For the mn^{th} impedance matrix term, vector potentials A_{mn} and F_{mn} are evaluated by integrations (4) and (6) over the shaded current source regions.

B. Testing Functions

Testing vector functions at the mth edge are defined as ℓ_m^+ and ℓ_m^-, as shown in Fig. 3. ℓ_m^+ extends from the T_m^+ centroid to the midpoint of the mth edge; ℓ_m^- extends from the midpoint of the mth edge to the T_m^- centroid.
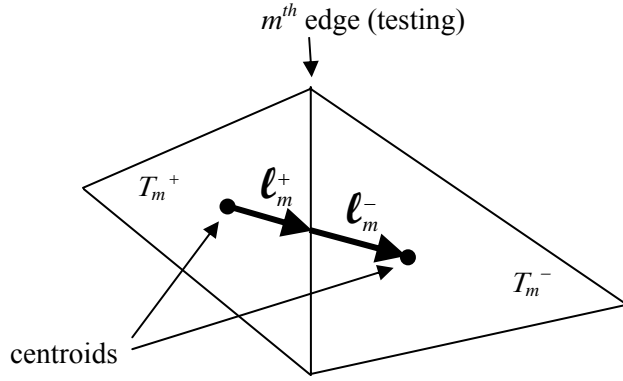
Fig. 3. Testing vectors at the mth edge.

Fig. 4. Observation points are the δ_m centroids for evaluation of A_{mn} and F_{mn}, the T_m centroids for evaluation of Φ_{mn}.

C. Testing Equations

In each of regions 1 and 2 (shown in Fig. 1), N testing equations (11) are written in matrix form to solve (1) and (2) for J and M at the patch edges $m = 1$ to N. For region 1, the right hand side of (11) has assigned nonzero values for the incident field; in region 2, the right hand side is zero because there is no incident field inside the scatterer.

$$\sum_{n=1}^{N}\left[j\omega A_{mn}^{+} \bullet \ell_m^{+} + j\omega A_{mn}^{-} \bullet \ell_m^{-} + \Phi_{mn}^{-} - \Phi_{mn}^{+} \right]$$
$$+ \sum_{n=1}^{N}\left[\frac{1}{\varepsilon}\nabla \times F_{mn}^{+} \bullet \ell_m^{+} + \frac{1}{\varepsilon}\nabla \times F_{mn}^{-} \bullet \ell_m^{-} \right] \quad (11)$$
$$= E_m^{i+} \bullet \ell_m^{+} + E_m^{i-} \bullet \ell_m^{-} .$$

[2] and [6] describe more details of triangular patch modeling with RWG basis functions; [1] further explains the implementation of unit pulse vector basis functions.

D. Observation and Source Points for Potential Evaluation

For the mn^{th} impedance matrix term, vector potentials A_{mn} and F_{mn} are evaluated as observed from the centroids of the δ_m^{+} and δ_m^{-} triangles. These triangles are defined by nodes at the T_m^{+} and T_m^{-} centroids and the endpoints of the mth edge, shown in Fig. 4.

For the mn^{th} impedance matrix term, scalar potential Φ_{mn} is evaluated as observed from the centroids of the T_m^{+} and T_m^{-} triangles, shown in Fig. 4. The source region is the entirety of the T_n^{+} and T_n^{-} triangles shown in Fig. 2.

E. Calculation of Potential Terms

A is calculated by a straightforward application of (4) with G computed numerically.

Φ is calculated from (5), making use of the Divergence Theorem. We assume that, everywhere in T_n, Φ_n is the divergence of A through the three sides of the T_n triangle.
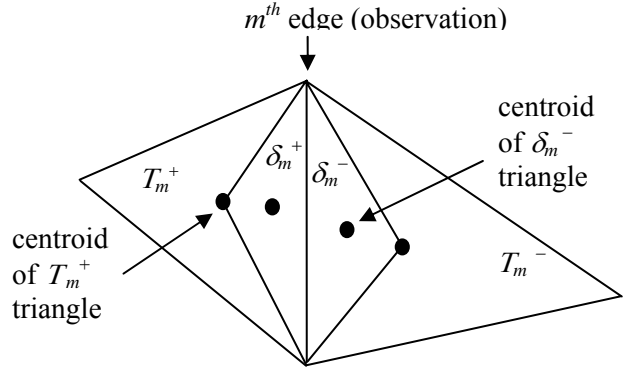
That divergence is calculated as

$$\nabla \bullet A = \left(J_1 L_1 + J_2 L_2 + J_3 L_3 \right)\int_T G dS \quad (12)$$

where L_1, L_2, and L_3 are the lengths of the sides of the T_n triangle and J_1, J_2, and J_3 are the scalar current components normal to those sides. Application of the testing functions has eliminated the necessity to compute $\nabla \Phi$ because the dot product of the testing vector with $\nabla \Phi$ reduces to $\Delta \Phi$ over the testing path.

$\nabla \times \dfrac{1}{\varepsilon}F$ is evaluated as follows:

$$\nabla \times \frac{1}{\varepsilon}F = \nabla \times \frac{1}{4\pi}\int_S M \cdot G dS$$
$$= \frac{1}{4\pi}\int_S \nabla G \times M dS \quad (13)$$
$$= \begin{cases} -\hat{n}\times\dfrac{M}{2} & \text{self terms} \\ \dfrac{1}{4\pi}\displaystyle\int_S \nabla G \times M dS & \text{non self terms} \end{cases}$$

where S is the shaded area depicted in Fig. 2. This "deleted integral" formulation follows from evaluating the Cauchy principal value for the singular self terms when, as in our case of δ_m centroid evaluation, the observation point is not on a patch edge [7].

F. Incident E-field

The incident E-field is evaluated at the δ_m^{+} and δ_m^{-} centroids, which are located two thirds of the way along the ℓ_m^{+} testing path and one third of the way along the ℓ_m^{-} testing path.

IV. NUMERICAL RESULTS

Examples are shown of scattering calculations for the canonical shapes of a sphere, a finite cylinder, and a cube. These geometries are represented in Fig. 5. In each case, an incident plane wave is assumed to be x-polarized, traveling in the +z direction. The pulse basis vector results are compared to results of calculations by other methods.
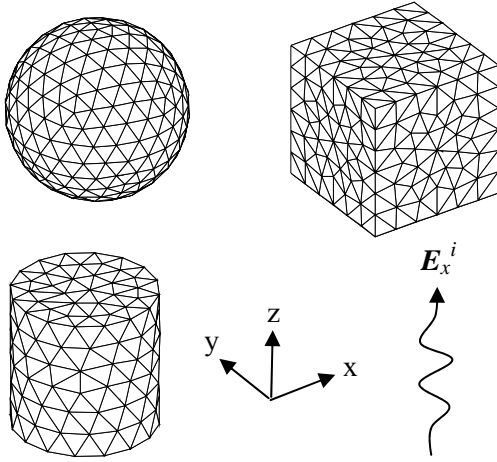

Fig. 5. RCS has been calculated for a dielectric sphere, a dielectric cylinder, and a dielectric cube separately.

A. Sphere

A dielectric sphere having diameter = 0.2 λ and $\varepsilon_R = 4$ is meshed with 500 triangles (750 edges) as shown in Fig. 5. The bistatic RCS is shown versus θ for observation angles $\phi = 0^\circ$ (Fig. 6) and $\phi = 90^\circ$ (Fig. 7). These results are compared with the analytic Mie series results [8].

B. Cylinder

A dielectric cylinder having diameter = 0.2 λ, height = 0.2 λ, and $\varepsilon_R = 3$ is meshed with 320 triangles (480 edges) as shown in Fig. 5. The bistatic RCS is shown versus θ in Figs. 8 and 9. These results are compared with body of revolution (BOR) MoM results.

C. Cube

A dielectric cube having side length = 0.2 λ and $\varepsilon_R = 4$ is meshed with 480 triangles (720 edges) as shown in Fig. 5. The bistatic RCS is shown versus θ in Figs. 10 and 11. These results are compared with surface integral equation (SIE) and volume integral equation (VIE) MoM results reported by Sarkar et al. [9]. Sarkar's SIE formulation used 192 triangles (288 edges), while the VIE formulation used 512 cubes.

D. Discussion

For the examples of dielectric sphere, cylinder, and cube, the paired pulse basis expansion functions produce RCS values very comparable to those values determined by other accepted methods. As the modeling mesh is made finer to increase spatial resolution, pulse results converge to the expected values. Although real values of ε have been used in the examples, complex values may be used to model a lossy dielectric or conductive material. The paired pulse basis vector solution method may also be extended to include collections of scatterers, composite dielectric/conducting bodies, or bodies composed of numerous regions of constant permittivity and permeability.

V. CONCLUSION

A pair of orthogonal unit pulse basis vector functions has been applied to the solution of MoM scattering problems for three-dimensional dielectric objects in the shapes of a sphere, a finite cylinder, and a cube. Good agreement was obtained between these results and the results from other analytic and numerical methods. These results indicate that the paired pulse basis vector method can be used for arbitrarily-shaped bodies, given a triangular mesh resolution appropriate for the electrical size of the body. The orthogonal spatial relationship between the electric and magnetic current basis functions should provide stable solutions for problems involving single, multiple, or hybrid dielectric/conducting bodies. Although other methods may give more accurate results for specific geometries, such as the Mie series method for a sphere or the BOR method for a cylinder, the paired pulse basis function method in combination with triangular surface patches will give good answers for many different geometries with fewer computations than the volume integration method.
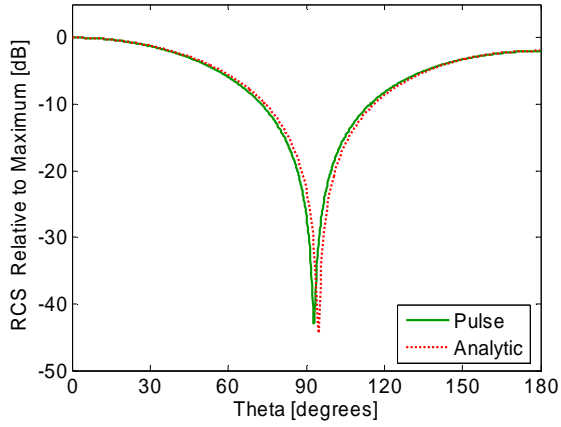
Fig. 6. Bistatic RCS at $\phi = 0°$ for a dielectric sphere, $\varepsilon_R = 4$. Pulse method (500 triangles) vs. Mie series method.
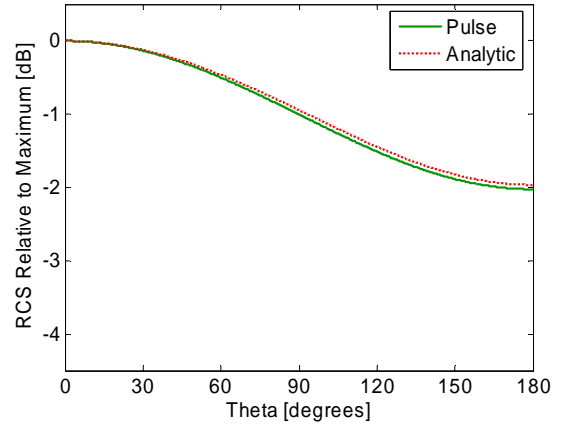

Fig. 7. Bistatic RCS at $\phi = 90°$ for a dielectric sphere, $\varepsilon_R = 4$. Pulse method (500 triangles) vs. Mie series method.
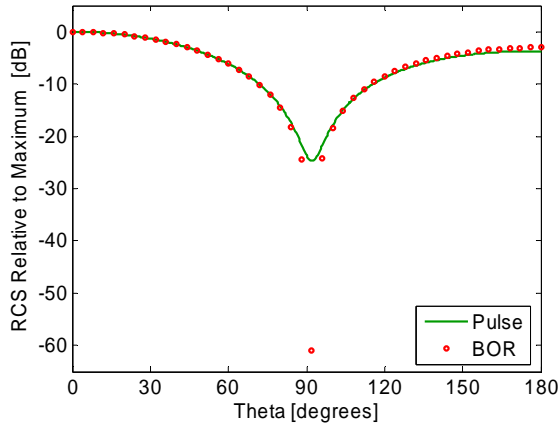

Fig. 8. Bistatic RCS at $\phi = 0°$ for a dielectric cylinder, $\varepsilon_R = 3$. Pulse method (320 triangles) vs. BOR method.
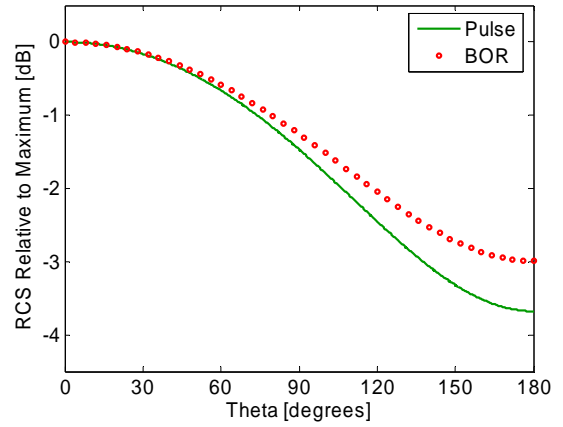

Fig. 9. Bistatic RCS at $\phi = 90°$ for a dielectric cylinder, $\varepsilon_R = 3$. Pulse method (320 triangles) vs. BOR method.
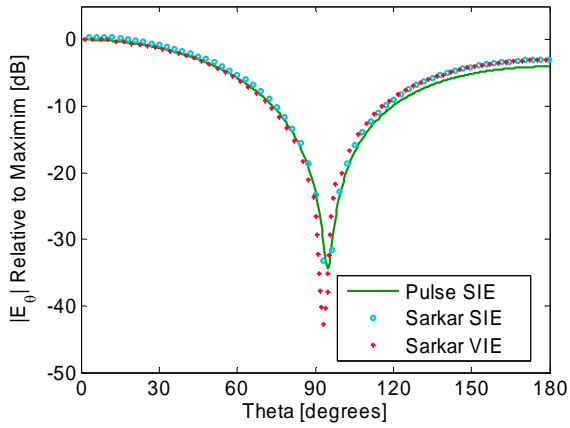

Fig. 10. Bistatic RCS at $\phi = 0°$ for a dielectric cube, $\varepsilon_R = 4$. Pulse method (480 triangles) vs. Sarkar's SIE method (192 triangles) and Sarkar's VIE method (512 cubes) [8].

Fig. 11. Bistatic RCS at $\phi = 90°$ for a dielectric cube, $\varepsilon_R = 4$. Pulse method (480 triangles) vs. Sarkar's SIE method (192 triangles) and Sarkar's VIE method (512 cubes) [8].
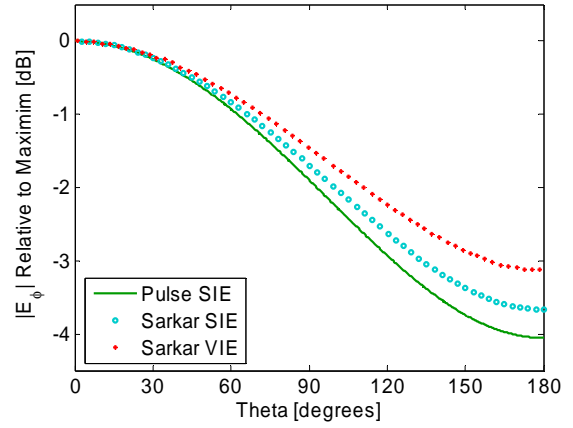
REFERENCES

[1] A. I. Mackenzie, M. E. Baginski, and S. M. Rao, "New basis functions for the electromagnetic solution of arbitrarily-shaped, three dimensional conducting bodies using method of moments," *The 23rd Annual Review of Progress in Applied Computational Electromagnetics*, March 19-23, 2007, Verona, Italy.

[2] S. M. Rao, D. R. Wilton, and A. W. Glisson, "Electromagnetic scattering by surfaces of arbitrary shape," *IEEE Transactions on Antennas and Propagation*, vol. AP-30, no. 3, pp. 409-418, May 1982.

[3] A. W. Glisson and D. R. Wilton, "Simple and efficient numerical methods for problems of electromagnetic radiation and scattering from surfaces," *IEEE Transactions on Antennas and Propagation*, vol. AP-28, no. 5, September 1980.

[4] B. Z. Steinberg and Y. Leviatan, "On the use of wavelet expansions in the method of moments," *IEEE Transactions on Antennas and Propagation*, vol. 41, no. 5, pp. 610-619, May 1993.

[5] L. C. Trintinalia and H. Ling, "An improved triangular patch basis for the method of moments," *IEEE Antennas and Propagation Society International Symposium*, 2000.

[6] S. M. Rao and D. R. Wilton, "E-field, H-field, and combined field solution for arbitrarily shaped three dimensional dielectric bodies, *Electromagnetics*, vol. 10, no. 4, pp. 407-421, 1990.

[7] J. Van Bladel, *Electromagetic Fields*, Hemisphere Publishing Corporation, New York, pp. 354-355, 1985.

[8] R. F. Harrington, *Time Harmonic Electromagnetic Fields*, McGraw-Hill Book Company, New York, pp. 289-298, 1961.

[9] T. K. Sarkar, E. Arvas, and S. Ponnapalli, "Electromagnetic scattering from dielectric bodies," Communication in *IEEE Transactions on Antennas and Propagation*, vol. 37, no. 5, pp. 673-676, May 1989.